Title
Optical and Power Characteristics of Synchrotron Radiation Sources

Journal
Optical Engineering, 34(2)

Author
Kim, K.-J.

Publication Date
1995-02-01

LBL-36840
UC-414
Preprint

Lawrence Berkeley Laboratory
UNIVERSITY OF CALIFORNIA

Accelerator & Fusion Research Division

Submitted to Optical Engineering

Optical and Power Characteristics of Synchrotron Radiation Sources

K.-J. Kim

February 1995

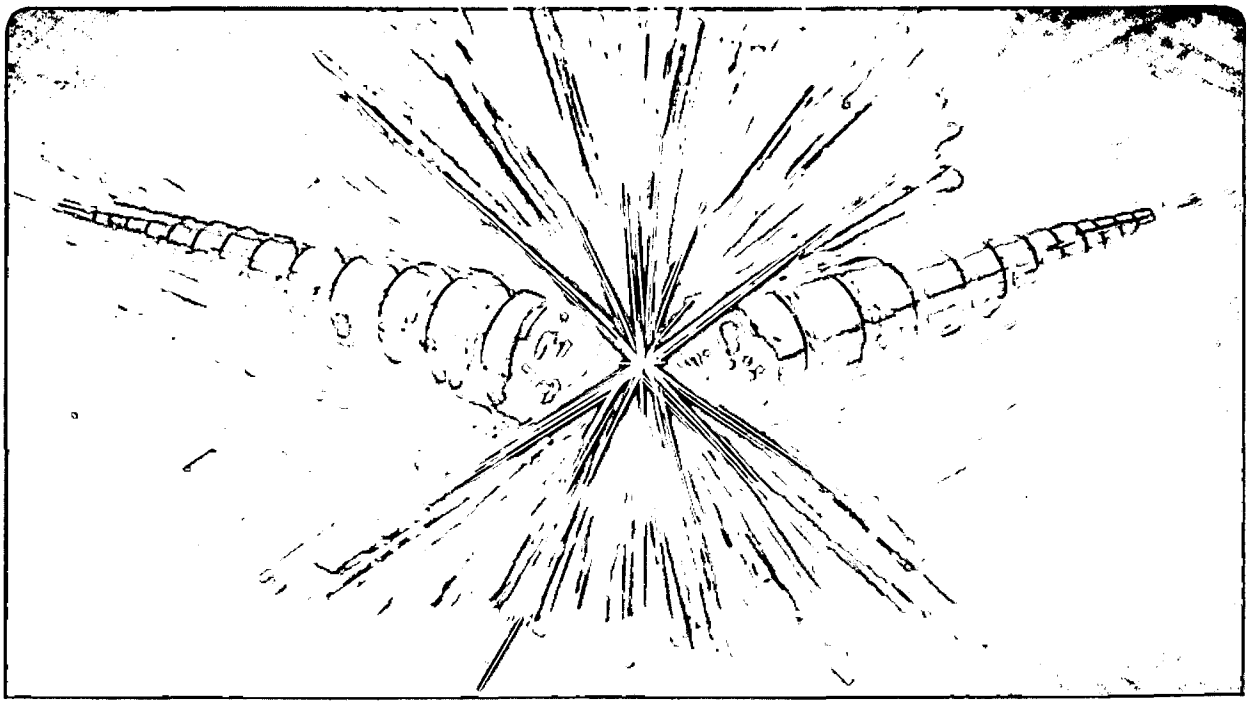

Prepared for the U.S. Department of Energy under Contract Number DE-AC03-76SF00098

DISCLAIMER

LBL-36840
UC-414

Optical and Power Characteristics of Synchrotron Radiation Sources

Kwang-Je Kim

Center for Beam Physics
Accelerator and Fusion Research Division
Lawrence Berkeley Laboratory
University of California
Berkeley, California 94720

February 1995

This work was supported by the Director, Office of Energy Research, Office of Basic Energy Sciences, Materials Sciences Division and Advanced Energy Projects Division, of the U.S. Department of Energy under Contract No. DE-AC03-76SF00098.

ABSTRACT

The optical and the power characteristics of various synchrotron radiation sources are summarized. The optical characteristics - flux, brightness, coherence, polarization, etc. — determine the quality of the source for photon experiments. The power characteristics determine the heat load on beam line elements. After discussing the cases for the bending magnet, wiggler and undulator, the case for the helical undulator is considered separately emphasizing its different power characteristics from the planar case.

1. INTRODUCTION

Synchrotron radiation — the radiation produced by a charged particle moving with relativistic speed in curved trajectories — provides an intense, tunable, bright sourse of photons in a wide spectral region from a few eV to tens of keV. It is becoming an indispensible tool in many areas of basic and applied sciences, as witnessed by the construction and/or completion of several advanced dedicated synchrotron radiation facilities around the world. In this paper, we review the characteristics of synchrotron radiation sources.

The unique property of synchrotron radiation has its origin in the fact that, for an extreme relativistic electron moving toward a stationary observer, the motion appears to occur in a time scale shorter by a factor γ^2 than that of the real motion[1,2]. Here, $\gamma = E_e/m_ec^2$, E_e the electron's relativistic kinetic energy, m_e its mass, and c the speed of light. In practical units

$$\gamma = 1957\ E_e\ [\mathrm{GeV}] \quad .$$

For typical synchrotron radiation sources, E_e ranges from about one to ten GeV, corresponding to the value of γ from 3000 to 30,000.

Synchrotron radiation is generated when extreme relativistic electrons are forced to make a curved trajectory through powerful magnetic fields. Three kinds of magnets are used to make such fields in synchrotron radiation sources: bending magnets, wigglers, and undulators. In bending magnets, electrons move in a simple circular trajectory. The emitted radiation is intense, with a very narrow angular divergence of about γ^{-1} around the trajectory plane, and has a broad energy spectrum centered around a few to a few tens of KeV. Wigglers can be regarded as a sequence of bending magnets of alternate polarities. Thus, its radiation characteristics are similar to those from bending magnets, apart from a 2N-fold enhancement of the intensity, where 2N is the number of the poles. An undulator is an N-period magnetic structure producing a gentle, periodic orbit. Because of the interference of radiation from different parts of the trajectory, the undulator radiation is squeezed into a discrete spectrum and narrower emission angles. The result is an N^2-fold enhancement of the angular density of the flux in the forward direction. The spectral characteristics of radiation from bending magnets, wigglers and undulators are illustrated and compared in Fig. 1-1.

Due to their high intensity and narrow angular divergence, the x-ray beams from synchrotron radiation sources are optically very bright, making them a valuable tool for scientific investigation. On the other hand, the high power density of the beams places a severe burden in the design of downstream optical elements. The generated x-ray beams can contain several kW of power confined to an angle less than one tenth of a miliradians. Some or most of this power is absorbed by the optical components that are used to confine, define, mask, reflect, focus, or monochromatize the beam. These components can be subjected to heat loads of several kW and heat fluxes in excess of 100 W/mm^2 as discussed elsewhere in this volume. Design of suitable cooled optical elements is necessary to fully expoit the generated x-ray beams. In fact, the deformation of optical

elements under the high heat loads must be kept to very low levels in order to prevent the angular spread or degradation of the very narrow, finely tuned, beam so deliberately produced. Thus, in view of the difficulties in the thermal management of high heat load x-ray components, it is instructive to include thermal load as one of the criteria used in the selection and design of x-ray generating devices. Concurrently, development of devices that can produce the desired photons without substantial parasitic power must be pursued.

Section 2 is an introduction to the various quantities characterizing the source properties. These are the brightness, flux and polarization which are important from the point of view of photon users, and the power which is important from the point of view of the beam optical line designers. Sections 3, 4 and 5 contain a brief review discussion of the characteristics of bending magnets, wigglers, and undulators, respectively. A more detailed treatment can be found, for example, in references [3,4,5]. Section 6 contains some new material concerning helical undulator radiation, in particular its power characteristics .

2. QUANTITIES CHARACTERIZING RADIATION SOURCES

2.1 Brightness and Flux. A fundamental characteristic of a radiation source is the density of photon flux in phase space[6,7,8]. The coordinates of the phase space is denoted by the pair $(\mathbf{x},\phi)$, where $\mathbf{x}$ and ϕ are respectively the position and the direction. In components, we have

$$\mathbf{x} = (x,y) \quad , \quad \phi = (\phi,\psi) \quad , \tag{2.1}$$

where x and y are the horizontal and the vertical positions, and ϕ and ψ are the horizontal and vertical angles, respectively. The distribution of the photon flux F in phase space is called the brightness function, and is given by

$$B(\mathbf{x},\phi) = \frac{d^4F}{d^2\mathbf{x}d^2\phi} \tag{2.2}$$

The brightness function evalutated at the origin will be simply referred to as the brightness B. It uniquely characterizes the strength of a radiation source because it is invariant under propagation through optical elements, such as lenses or free space[6].

Integrating the brightness function over the angles or positions, we obtain the angular or the spatial density of flux:

$$\frac{d^2F}{d^2\phi} = \int B(\mathbf{x},\phi)\, d^2\mathbf{x} \quad , \tag{2.3}$$

$$\frac{d^2F}{d^2\mathbf{x}} = \int B(\mathbf{x},\phi)\, d^2\phi \quad . \tag{2.4}$$

Finally, one obtains the total flux by integration, as follows:

$$F = \int \frac{d^2F}{d^2\mathbf{x}} d^2\mathbf{x} = \int \frac{d^2F}{d^2\phi} d^2\phi = \int B(\mathbf{x},\phi;z)\, d^2\mathbf{x}d^2\phi \quad . \tag{2.5}$$

The flux is another invariant.

The various differential fluxes in the above are understood to be spectral quantities, i.e., the fluxes in a small bandwidth around a given frequency. To be precise, therefore, we should call B the spectral brightness, $d^2F/d^2\phi$, the angular density of spectral flux, and so on. However, we often drop the adjective spectral for the sake of brevity.

For practical calculations, the following units for the spectral flux and brightness are commonly used

$$B = \frac{\text{number of photons}}{(\text{s})\,(\text{mm}^2)\,(\text{mr}^2)\,(0.1\%\ \text{bandwidth})} \tag{2.6}$$

$$F = \frac{\text{number of photons}}{(\text{s})(0.1\%\ \text{bandwidth})} \tag{2.7}$$

Figure 2-1 shows the spectral brightness for several synchrotron radiation sources. For undulators, each curve is the locus of sharp peaks that can be tuned by changing the undulator gaps.

2.2 Coherence. Another important characteristics of the photon beams is its coherence, which is a measure of the degree to which the radiation can exhibit interference patterns. Two types of coherence can be distinguished: The transverse (or spatial) coherence refers to the coherence of electromagnetic vibrations at two points perpendicular to the propagation direction. The longitudinal (or temporal) coherence refers to the case of two points along the propagation direction. Photons within the phase space area $\lambda/2$, where λ is the radiation wavelength, are transversly coherent. Since there are two transverse dimensions, the transversely coherent flux is given by

$$F_{coh,T}=B(\lambda/2)^2 \tag{2.8}$$

The temporal coherence is characterized by the coherence length l_c which is related to the bandwidth $\Delta\lambda/\lambda$ by

$$l_c=\lambda(\lambda/\Delta\lambda)=\lambda^2/\Delta\lambda \tag{2.9}$$

2.3 Polarization An important characteristerization of radiation is the polarization. Synchrotron radiation offers a variety of polarization; linear, circular, or elliptical.

2.4 Power. The brightness and flux are the quantities relevant for planning photon experiments. In designing an optical transport system from a source to an experimental chamber, called the beam line, it is also important to know the output of the power integrated over all frequencies. This will be refered to as the power, P, throughout this paper. The angular distribution of the power is denoted by $dP/d^2\phi$. The synchrotron radiation beam lines, especially in high energy facilities for x-rays, have to be designed to handle tens of kW of power emitted by the sources.

3. BENDING MAGNET RADIATION

For an electron following a circular trajectory (as in the bending magnets of a storage ring) the bending radius, in the extreme relativistic case, is given by

$$\rho = \frac{E_e}{ecB} \quad , \tag{3.1}$$

where B is the magnetic field strength. In practical units this becomes

$$\rho[m] = 3.3\ E_e\ [GeV]/B\ [T] \quad .$$

The bending-magnet radiation has a smooth spectral distribution, with a broad maximum near the critical frequency ω_c given by

$$\omega_c = \frac{3\gamma^3 c}{2\rho} \quad . \tag{3.2}$$

The photon energy corresponding to ω_c, is $\varepsilon_c = \hbar\omega_c$, which in practical units is

$$\varepsilon_c\ [keV] = 0.665\ E_e^2\ [GeV]\ B\ [T] \quad .$$

3.1 Angular Density of Flux. The angular density of the spectral flux is given by[1]

$$\frac{d^2F}{d^2\phi} = \frac{3\alpha}{4\pi^2}\gamma^2\frac{\Delta\omega}{\omega}\frac{I}{e}\left[\frac{I}{e}\right]^2\left(1+X^2\right)^2\left[K_{2/3^2}(\eta)+\frac{X^2}{1+X^2}K_{1/3^2}(\eta)\right] \quad . \tag{3.3}$$

where α is the fine structure constant, ω the angular frequency of the radiated photons, I the electron beam current, the subscripted K's are modified Bessel functions of the second kind, and

$$\eta = \frac{1}{2}\frac{\omega}{\omega_c}(1+X^2)^{3/2} \quad , \tag{3.4}$$

$$X = \gamma\psi \quad , \tag{3.5}$$

In the horizontal direction, $\psi = 0$, Eq.(3.3) becomes in practical units [photons $\cdot$ s^{-1} $\cdot$ mr^{-2}

(0.1% bandwidth)$^{-1}$],

$$\frac{d^2F}{d^2\phi}\Big|_{\psi=0} = 1.33\times10^{13}\, E_e^2[\mathrm{GeV}]I[\mathrm{A}]H_2(\omega/\omega_c) \quad , \tag{3.6}$$

where

$$H_2(y) = y^2K_{2/3}^2(y/2) \quad . \tag{3.7}$$

The function $H_2(y)$ is plotted in Fig. 3-1. The distribution integrated over the vertical angle is given by

$$\frac{dF}{d\phi} = \frac{\sqrt{3}}{2\pi}\alpha\gamma\frac{\Delta\omega}{\omega}\frac{I}{e}\frac{\omega}{\omega_c}\int_{\omega/\omega_c}^{\infty} K_{5/3}(y')dy' \quad . \tag{3.8}$$

In practical units [photons $\cdot$ s^{-1} $\cdot$ mr^{-1} $\cdot$ (0.1% bandwidth)$^{-1}$],

$$\frac{dF}{d\phi} = 2.46\times10^{13}\, E_e\,[\mathrm{GeV}]\, I\,[\mathrm{A}]\, G_1(\omega/\omega_c) \quad ,$$

where

$$G_1(y) = y\int_y^{\infty} K_{5/3}(y')\,dy' \quad . \tag{3.9}$$

The function $G_1(y)$ is also plotted in Fig. 3-1.

If the angular distribution in ψ were of Gaussian shape, then the rms divergence σ_ψ can be calculated by taking the ratio of Eq. (3.8) and Eq. (3.3) evaluated at $\psi = 0$:

$$\sigma_\psi = \sqrt{\frac{2\pi}{3}}\frac{1}{\gamma}\left[\frac{\omega}{\omega_c}\right]^{-1}\frac{\int_{\omega/\omega_c}^{\infty} K_{5/3}(y)dy}{K_{2/3}^2(\omega/2\omega_c)} \quad . \tag{3.10}$$

In reality, the distribution is not Gaussian, especially in view of the fact that the distribution for the vertically polarized component vanishes in the horizontal direction

$\psi = 0$. However, σ_ψ defined by Eq. (3.10) is still a simple and useful measure for the angular divergence. Eq. (3.10) is of the form

$$\sigma_\psi = \frac{1}{\gamma} C(\omega/\omega_c) \quad . \tag{3.11}$$

The function C(y) is plotted in Fig. 3-2. At the critical energy σ_ψ becomes $0.64/\gamma$.

3.2 Polarization. Radiation from a bending magent is linearly polarized when observed in the bending plane. Out of this plane, the polarization is elliptical and can be decomposed into its horizontal and vertical components. The first and the second terms in the last bracket of Eq. (3.3) correspond, respectively, to the intensity of the horizontally and vertically polarized components. Fig. 3-3 gives the normalized intensities of these two components, as functions of emission angles, for different energies. the square root of the ration of these intensities is the ratio of the major and minor axes of the polarization ellipse. The sense of the electric field rotation reverses as the vertical observation angle changes from positive to negative.

3.3 Brightness. To compute the brightness, we first evaluate the diffraction limted source size corresponding to the divergence angle σ_ψ:

$$\sigma_r = \lambda/(4\pi\sigma_\psi) \quad . \tag{3.12}$$

To simplify the calculation, we neglect the effect of the curvature of the electron trajectory on the effective source size. The expression for the bending-magnet brightness then becomes

$$B = \left.\frac{d^2F}{d\phi d\psi}\right|_0 / 2\pi \left[\left(\sigma_x^2 + D^2\,\sigma_\varepsilon^2 + \sigma_r^2\right) \left(\sigma_y^2 + \sigma_r^2 + \frac{\varepsilon_y^2 + \epsilon_y \gamma_y \sigma_r^2}{\sigma_\psi^2} \right) \right]^{1/2} \quad . \tag{3.13}$$

In the above , γ_y is the third betatron function in the y direction, ε_y is the beam emittance, D is the dispersion function in the x direction, σ_ε is the rms value of the relative energy spread, and σ_x (σ_y) is the rms electron beam size in the x(y) direction. It is assumed that the electrons' angular divergence is much smaller than σ_ψ. Notice that the nonvanishing dispersion function in the bending magnet contributes to an additional term in the effective source size proportional to the energy spread.

3.4 Power The angular distribution of the power in bending magnet radiation is given by[1]

$$\frac{d^2P}{d^2\phi} = \frac{d^2P}{d^2\phi}\bigg|_0 \frac{1}{(1+\gamma^2\psi^2)^{5/2}}\left[1 + \frac{5}{7}\frac{\gamma^2\psi^2}{1+\gamma^2\psi^2}\right] . \tag{3.14}$$

Here

$$\frac{d^2P}{d^2\phi}\bigg|_0 = \frac{7}{64\pi}\frac{e^2}{\varepsilon_0}\frac{\gamma^5}{\rho}\frac{I}{e} = \frac{7}{64\pi}\frac{e^2}{\varepsilon_0}\frac{eB}{m_e c}\gamma^4\frac{I}{e} . \tag{3.15}$$

is the power density in the forward direction. In units of $W \cdot mr^{-2}$, this becomes

$$\frac{d^2P}{d^2\phi}\bigg|_0 = 5.42\ B\,[T]\ E_e^4\,[GeV]\ I\,[A]$$

In Eq. (3.14), the first and second terms in the last bracket correspond to, respectively, the power of the horizontally and vertically polarized components. Integrating Eq. (3.14) over the angles, we obtain

$$P = \frac{2}{3}\frac{e^2}{4\pi\varepsilon_0}\frac{I}{e}\frac{\gamma^4}{\rho^2}\ell \tag{3.16}$$

Here $\ell = \rho\Delta\phi$ is the length of the arc. The contribution of the horizontally polarized component to the total power is seven times that from the vertically polarized component. In practical units, the total emitted power is

$$P\,[kW] = 1.27\ E_e^2\,[GeV]\ B^2\,[T]\ I\,[A]\ \ell\,[m] . \tag{3.17}$$

4. WIGGLER RADIATION

4.1 Periodic Magnetic Structures. Wigglers and undulators are periodic magnetic structures operating in the straight sections of storage rings and are collectively known as insertion devices. Short–period–length insertion devices producing high magnetic fields are usually constructed from permanent magnets after the pioneering work by K. Halbach[9]. The magnetic field B in most of these devices is in the vertical direction and varies sinusoidally:

$$B_y = -B_o \sin(2\pi z/\lambda_w) \quad , \quad 0 \le z \le N\lambda_w \quad . \tag{4.1}$$

Here B_o is the peak magnetic field, λ_W is the period length and N the number of periods. By integrating the equation of motion, the electron's transverse velocity $c\beta_x$ is found to be

$$\beta_x = \frac{K}{\gamma}\cos(2\pi z/\lambda_w) \quad . \tag{4.2}$$

Here

$$K = eB_o\lambda_w/2\pi mc = 0.934\ \lambda_w[\text{cm}]\ B_o[\text{T}] \tag{4.3}$$

is a dimensionless quantity referred to as the deflection parameter. The maximum slope of the trajectory is

$$\delta = \frac{K}{\gamma} \quad .$$

A typical insertion device, based on a permanent–magnet–steel hybrid design, is schematically illustrated in Fig. 4-1.

4.2 Radiation Characteristics. In a wiggler, K is large (typically > 10) and radiation from different parts of the electron trajectory adds incoherently. The angular density of flux or power is then given by 2N (where N is the number of magnet periods) times the

appropriate formula for bending magnets. However, ρ or B must be taken at the point of the electron's trajectory tangent to the direction of observation. Thus the critical energy for a horizontal angle ϕ is given by

$$\varepsilon_c(\phi) = \varepsilon_{c\,max}\sqrt{1-(\phi/\delta)^2}\quad , \tag{4.4}$$

where

$$\varepsilon_{cmax} = 0.655E^2[\mathrm{GeV}]B_0[\mathrm{T}]\,.$$

Calculation of the brightness for wiggler radiation must take into account the depth-of field effects -- the contribution to the apparent source size from different poles. The peak brightness for wiggler radiation is given by

$$B = \frac{d^2F}{d^2\phi}\sum_{\pm,n}\frac{1}{2\pi}\frac{\exp\left[-\frac{1}{2}\frac{x_0^2}{\sigma_x^2+z_{n\pm}^2\sigma_{x'}^2}\right]}{\left[\left(\sigma_x^2+z_{n\pm}^2\sigma_{x'}^2\right)\left[\frac{\varepsilon_y^2}{\sigma_{x'}^2}+\sigma_y^2+z_{n\pm}^2\sigma_{y'}^2\right]\right]^{1/2}}\quad ,$$

$$z_{n\pm} = \lambda_w\left[n\pm\frac{1}{4}\right]\quad . \tag{4.5}$$

In the above, σ_x and $\sigma_{x'}$ (σ_y and $\sigma_{y'}$) are the rms transverse size and angular divergence of the electron beam in the x direction (the y direction), respectively. The sum is over the contributions from different poles. $Z\pm n$ are the z-coordinates of the points where the electron trajectory is tangent to the forward direction. Note that there are two points (one from each pole specified by ±) per each period. The phase space distribution of wiggler radiation is illustrated in Fig. 4-2. The the contribution of the central pole is indicated by the upright ellipse. The contributions from other poles, when projected onto the central pole position, are a set of sheared ellipses. The high brightness part of the distribution occurs in a small region near the origin where the contribution from different poles

overlap each other. The exponential factor in Eq. (4.5) arises because wigglers have two source points, separated by $2x_0$, where

$$x_0 = \frac{K}{\gamma}\frac{\lambda_w}{2\pi} \quad . \tag{4.6}$$

4.3 Polarization. In contrast to the bending magnet radiation, which is elliptically polarized away from the horizontal direction, the polarization of radiation from an electron moving in a planar trajectory given by Eq. (4.1) is always linear. This is due to the interference of radiation amplitudes from two poles in each period. However, the direction of polarization in wiggler radiation in the limit of a large deflection parameter K changes very rapidly as a function of the vertical angle. Thus, the radiation collected over a small angular interval is effectively partially polarized with the degree of polarization given by

$$P_{pol} = \frac{(1+X^2)\, K_{2/3}^2(\eta) - X^2\, K_{1/3}^2(\eta)}{(1+X^2)\, K_{2/3}^2(\eta) + X^2\, K_{1/3}^2(\eta)} \quad . \tag{4.7}$$

The quantities appearing in the RHS of Eq. (4.7) are defined in Section 4.2.

4.4 Power. The power from a wiggler can be obtained either from the bending magnet formulae given in Section 3.4, or from a large K limit of the undulator formulae as discussed in Section 5.3.

5. UNDULATOR RADIATION

When the deflection parameter K is of order unity or less, radiation from different periods can coherently interfere, thus producing sharp peaks at harmonics of the fundamental. In this case, the device is called an undulator. In this section, we consider the case of the

planar undulator[10], in which the electron trajectory is described by the formulae in Section 4.1. However, we will use the subscript u, for example λ_u rather than λ_w in the case of an undulator. The case of the helical undulator is considered in the next section.

5.1 Spectral and Anglular Distritribution[10,11,12]. We consider first the case where effects due to emittance can be neglected. The frequency of the fundamental on axis ($\phi = \psi = 0$) is

$$\omega_1(0) = \left(\frac{2\gamma^2}{1 + K^2/2}\right) \omega_u \ , \tag{5.1}$$

where $\omega_u = 2\pi c/\lambda_u$. The corresponding energy in practical units is

$$\varepsilon_1[\text{keV}] = \frac{0.95\, E_e^2\,[\text{GeV}]}{(1 + K^2/2)\,\lambda_u[\text{cm}]} \ .$$

Away from the forward direction, at an angle $\theta = \sqrt{\phi^2 + \psi^2}$, the frequency becomes red-shifted:

$$\omega_1(\theta) = \omega_1(0)\, \frac{1}{1 + \gamma^2\theta^2/(1 + K^2/2)} \ . \tag{5.2}$$

The width of the spectral line (FWHM) near nth harmonic is

$$\left.\frac{\Delta\omega}{\omega_n}\right| = \frac{4.8}{\pi n N} \sim \frac{0.9}{nN} \ . \tag{5.3}$$

If the frequency is fixed at nth harmonic, the angular distribution has a narrow cone centered in the forward direction, called the *central cone*. The rms width of the central cone is given by

$$\sigma_{r'} = \frac{1}{2\gamma}\sqrt{\frac{1 + K^2/2}{nN}} = \sqrt{\frac{\lambda_n}{2L}} \ , \tag{5.4}$$

where $\lambda_n = \lambda_1/n$ is the wavelength corresponding to ω_n and $L = N\lambda_u$ is the length of the undulator. In addition, rings of radiation of the same frequency also appears at angular distances

$$\theta_{n\ell} = \frac{1}{\gamma}\sqrt{\frac{\ell}{n}(1 + K^2/2)} \quad (\ell = 1,2,3,...). \tag{5.5}$$

The angular structure of undulator radiation is illustrated in Fig. 5-1.

The peak angular density at nth harmonic is given by

$$\left.\frac{d^2F^n}{d^2\phi}\right|_0 = \alpha N^2\gamma^2 \frac{\Delta\omega}{\omega}\frac{I}{e}F_n(K) \quad (n = 1,3,5,...) \tag{5.6}$$

where

$$F_n(K) = \frac{K^2n^2}{(1 + K^2/2)^2}\left\{J_{\frac{n-1}{2}}\left[\frac{nK^2}{4(1 + K^2/2)}\right] - J_{\frac{n-1}{2}}\left[\frac{nK^2}{4(1 + K^2/2)}\right]\right\}^2 . \tag{5.7}$$

Here, the J's are Bessel functions. The function $F_n(K)$ is plotted in Fig. 5-2. In practical units [photons • s^{-1} • mr^{-1} • (0.1% bandwidth)$^{-1}$], Eq. (5.6) becomes

$$\left.\frac{d^2F^n}{d^2\phi}\right|_0 = 1.74 \times 10^{14}\, N^2 E_e^2\ [\text{GeV}]\ I[\text{A}]\ F_n(K) \ .$$

The flux contained in the central cone, F^n, is obtained by multiplying Eq. (5.6) by the area of the central cone $2\pi\sigma_{r'}^2$:

$$F^n = \frac{\pi}{2}\alpha N\frac{\Delta\omega}{\omega}\frac{I}{e}Q_n(K) \ , \tag{5.8}$$

where

$$Q_n(K) = (1 + K^2/2)\,F_n(K)/n \ . \tag{5.9}$$

The function $Q_n(K)$ is plotted in Fig. 5-3. In practical units [photons•s^{-1}•(0.1% bandwidth)$^{-1}$], Eq. (5.8) becomes

$$F^n = 0.72 \times 10^{14}\, N Q_n I[A] \quad .$$

It should be noted that the flux formula in the above is one half of those quoted in the previous publications [11,12]. This is because we have computed the flux at $\omega = n\omega_1(0)$; more flux is produced at slightly lower frequencies, and it becomes twice of that given by Eq. (5.8) at around $\omega = \omega_1(0)(n - N^{-1})$. At these frequencies, however, the angular distribution has a dip in the forward direction, and therefore the Gaussian approximation used in the present treatment does not apply.

In practical undulators, the deviation of the electron trajectory from the ideal sinusoidal curve due to magnet errors causes, in general, a reduction in the undulator performance[13]. In advanced synchrotron radiation facilities, the magnet errors are tightly controlled so that such a reduction is negligible for useful harmonics.

5.2 Brightness and Coherence of Undulator Radiation. The diffraction limited rms source size corresponding to Eq. (5.4) is

$$\sigma_r = \sqrt{2\lambda L}/4\pi \qquad (5.10)$$

Because Eqs. (5.4) and (5.10) give very small angular divergence and size, the brightness of the undulator radiation from an electron beam depends sensitively on the electrons' distribution. Electrons in storage rings are distributed in a finite area of transverse phase space - position times angle. We introduce the rms electron beam sizes σ_x (horizontal) and σ_y (vertical) and electron beam divergences $\sigma_{x'}$ (horizontal) and $\sigma_{y'}$ (vertical). The quantities $\varepsilon_x=\sigma_x\ \sigma_{x'}$ and $\varepsilon_y=\sigma_y\ \sigma_{y'}$ are known as the horizontal and vertical electron beam emittances, respectively. They are determined by the beam dynamics of the storage ring. The ratios $\beta_x=\sigma_x/\sigma_{x'}$ and $\beta_y=\sigma_y/\sigma_{y'}$ are known as the horizontal and vertical beta functions (the second Twiss parameter), respectively. They are determined by the magnetic lattice design of the storage ring. Taking into account the electron beam

emittance, the rms source size and the angular divergence in the x direction become, respectively,

$$\sigma_{Tx} = \sqrt{\sigma_r^2 + \sigma_x^2} \ , \tag{5.11}$$

$$\sigma_{Tx'} = \sqrt{\sigma_{r'}^2 + \sigma_{x'}^2} \tag{5.12}$$

and similarly for the y direction.

The total flux in the central cone remains unchanged, being given by Eq. (5.8). Thus, the peak angular density taking into account the electron beam distribution is[7,8,11]

$$\left.\frac{d^2F^{\,n}}{d^2\phi}\right|_0 = \frac{F^{\,n}}{2\pi\sigma_{Tx}\sigma_{Ty'}} \ . \tag{5.13}$$

The expression for the peak brightness becomes

$$B_0 = \frac{F}{(2\pi)^2\,\sigma_{Tx}\sigma_{Tx'}\sigma_{Ty}\sigma_{Ty'}} \ . \tag{5.14}$$

Examples of undulator brightness were shown in Fig. 2-1.

Using Eq. (2.8), the transversly coherent part of the undulator flux is

$$F_{coh,T} = \frac{\lambda^2 F}{(4\pi)^2\,\sigma_{Tx}\sigma_{Tx'}\sigma_{Ty}\sigma_{Ty'}} \ . \tag{5.15}$$

The factor multiplying F in the RHS of Eq. (5.15) is the coherent fraction. For coherence experiments involving diffraction in the vertical direction only, the coherent fraction is given by

$$\text{Vertical Coherence Fraction} = \lambda/(4\pi\,\sigma_{Ty}\sigma_{Ty'}) \ . \tag{5.16}$$

Since the vertical emittance is significantly smaller, up to a factor of 100, the vertical coherence fraction is quite high. Figure 5-4 shows the coherent fraction as a function of the photon energy for machine parameters corresponding to a typical third generation synchrotron radiation facility; $\varepsilon_x=10^{-8}$ m-rad, $\varepsilon_y=10^{-9}$ m-rad, $\beta_x=10$ m, and $\beta_x=4$ m. For a practical optical system, it is possible to use several radiation modes without significantly losing the resolution. Thus, the effective coherent fraction could be several times larger than that given by Eq. (5.15). The dotted line is the vertical coherent fraction.

The discussion in this subsection is based on the simple approximation that the phase space distribution of the undulator radiation can be represented by a product of Gaussian distributions. A more detailed study based on the Wigner distribution shows the deviation from the Gaussian distribution[14]. However, the approximation is nevertheless useful due to its simplicity.

5.3 Power. The angular distribution of radiated power from an undulator of deflection parameter K is given by[15]

$$\frac{d^2P}{d^2\phi} = \left.\frac{d^2P}{d^2\phi}\right|_0 \cdot f_K(\phi,\psi) \quad . \tag{5.17}$$

Here

$$\left.\frac{d^2P}{d^2\phi}\right|_0 = \left\{\frac{7}{64\pi}\,\frac{e^2}{\varepsilon_0 c}\,\gamma^4 K\omega_u\,\frac{I}{e}\right\} 2NG(K) \tag{5.18}$$

is the power density in the forward direction, with

$$G(K) = \frac{K\left(K^6 + \frac{24}{7}K^4 + 4K^2 + \frac{16}{7}\right)}{(1+K^2)^{7/2}} \quad . \tag{5.19}$$

The expression within the curly brackets in Eq. (5.18) is the same as the peak power density for the bending magnet, Eq. (4.15), if one replaces the bending field B by the peak undulator field B_0. The factor 2N accounts for the 2N poles in an N–period

undulator, and the factor G(K) accounts for the interference effect. The function G(K) is plotted in Fig. 5-5. From the plot, we see that the power density in the forward direction is less than that from a sequence of bending magnets due to the interference effect. However, G(K) is practically unity for $K \geq 2$. In practical units of $W \cdot mr^{-2}$, Eq. (5.18) becomes

$$\left.\frac{d^2P}{d^2\phi}\right|_0 = 10.84\, B_0[T]\, E^4[GeV]\, I[A]\, NG(K)$$

The angular function f_K in Eq. (5.17) is give by

$$f_K(\phi,\psi) = \frac{16K}{7\pi G(K)} \int_{-\pi}^{\pi} d\xi\, \frac{\sin^2\xi}{D^5} \left((1 + X^2 - Y^2)^2 + 4X^2Y^2\right) , \qquad (5.20)$$

where $X = \gamma\psi$, $Y = K \cos \xi - \phi\gamma$, and $D = 1 + X^2 + Y^2$. It describes the angular dependence with the normalization $f_K(0,0) = 1$. Figure 5-6 show the behavior of this function. When K becomes larger than 2, Eq. (5.20) approaches quickly to the function

$$f_\infty(\phi,\psi) = \sqrt{1 - (\gamma\phi/K)^2} \times \left\{ \frac{1}{\left(1 + (\gamma\psi)^2\right)^{5/2}} + \frac{5(\gamma\psi)^2}{7\left(1 + (\gamma\psi)^2\right)^{7/2}} \right\} . \qquad (5.21)$$

The factor within the curly brackets is the same as the angular distribution of the power from bending magnets, given by Eq. (3.14), while the factor $\sqrt{1 - (\gamma\phi/K)^2}$ arises because the magnetic field observed in the ϕ direction in a sinusoidal trajectory is reduced by that factor. In the limit $K \to 0$, one can derive from Eq. (5.18) that [16]

$$K \to 0 : f_K(\phi,\psi) = \frac{1 + 2\gamma^2(\psi^2 - \phi^2) + (\gamma^2(\phi^2 + \psi^2))^2}{(1 + \gamma^2(\phi^2 + \psi^2))^5} \qquad (5.22)$$

Integrating Eq. (5.17) over the solid angle, we find that the total power is given by

$$P = \frac{N}{6} \frac{e^2}{\varepsilon_0 c} \frac{I}{e} \omega_u \gamma^2 K^2 = \frac{e^2}{12\pi\varepsilon_0} \left(\frac{eB_0}{mc}\right)^2 \gamma^2 L \frac{I}{e} . \qquad (5.23)$$

This can be obtained from Eq. (3.16) by replacing $\ell \rightarrow L$ and $B^2 \rightarrow (1/2)B^2$. The factor 1/2 here accounts for the fact that the magnetic field is not constant but sinusoidal. In practical units, Eq. (5.23) becomes

$$P[kW] = 0.63\, E_e^2\, [GeV]\, B_o^2\, [T]\, I[A]\, L[m] \quad .$$

Undulators and wigglers in modern synchrotron radiation facilities are intense sources of thermal power–tens of kilowatts into a fraction of $mrad^2$ of a solid angle. The mechanical and optical elements of the beam lines need to be protected from the power by masks or by appropriate cooling arrangements. On the other hand, the useful part of the flux for undulators is confined to the cental cone given by Eq. (5.12), which for the current generation of machines optimized for UV and soft x-raysis much narrower than the angular openings of the thermal power profile. Thus the power load on optical elements in an undulator beam line is a small fraction of the total power. For high energy storage rings optimized for hard x-rays, however, the thermal power in the central cone could be 10-15% of the total power and thus still be too high. One possible way to avoidthe power problem is to employ a helical undulator discussed in the next section.

In this section, we have discussed the properties of a planar sinusoidal undulator. Recently Sasaki has proposed a new, quasi-periodic undulator to suppress higher harmonics[17].

6. HELICAL UNDULATOR

Planar insertion devices, which we have considered so far and in which all the pole faces are parallel, produce linear polarization. Circular or elliptical polarization can be produced by using different magnet arrangements [20,21,22,23,24]. Here, we discuss the helical undulator, first studied by Alferov et al., in their pioneering work on synchrotron

radiation [25]; and also by Kincaid[26]. In particular we write down expressions for various power characteristics which have not been discussed in detail so far[27].

In a helical undulator, the magnetic field is given by

$$(B_x, B_y) = B_o\,(-\sin(2\pi z/\lambda_u)\,,\ \cos(2\pi z/\lambda_u)\,),\quad 0 \le z \le N\lambda_u\ . \tag{6.1}$$

The spectrum in the forward direction is sharply peaked at the fundamental frequency given by Eq. (5.1) with $K^2/2$ replaced by K^2:

$$\omega_1(0) = \omega_u \frac{2\gamma^2}{1+K^2}.$$

In contrast to the case of a planar undulator, helical undulator does not produce higher harmonic radiation in the forward direction. However, harmonics are produced in other directions.

The angular density of the flux in the forward direction is given by

$$\left.\frac{d^2F}{d^2\phi}\right|_0 = \alpha N^2 \gamma^2 \frac{\Delta\omega}{\omega}\frac{I}{e}\frac{K^2}{1+K^2} \tag{6.2}$$

The angular distribution of the power from a helical undulator can be written in a form similar to Eq. (5.17):

$$\frac{d^2 P_H}{d^2\phi} = \left.\frac{d^2 P_H}{d^2\phi}\right|_0 f_K^H(\theta)\ , \tag{6.3}$$

where $\theta = \sqrt{\phi^2 + \psi^2}$ and

$$f_K^H(\theta) = \frac{(1+K^2)}{2\pi}\int_{-\pi}^{\pi} d\xi\,\frac{D^2 - 4\gamma^2\theta^2\sin^2\xi}{D^5}\ , \tag{6.4}$$

with

$$D = K^2 + \gamma^2\theta^2 + 1 - 2K\gamma\theta\cos\xi \tag{6.5}$$

The function f_K^H is normalized so that $f_K^H(0) = 1$. The power density in the forward direction is given by

$$\left.\frac{d^2P}{d^2\phi}\right|_0 = \frac{Ne^2}{\pi\varepsilon_0 c}\gamma^4\frac{I}{e}\omega_u\frac{K^2}{(1+K^2)^3} \tag{6.6}$$

Note that Eq. (6.6) vanishes as K becomes large. This is due to the fact that, as K becomes larger, most of the power is contained in higher harmonics which is forbidden in the forward direction. It turns out that the power distribution is peaked in the direction $\theta = K/\gamma$ for a large K. Thus, it is more convenient to write Eq. (6.3) as follows:

$$\frac{d^2P}{d^2\phi} = \left.\frac{d^2P}{d^2\phi}\right|_{\theta=K/\gamma} g_K^H(\theta)\ , \tag{6.7}$$

where

$$\left.\frac{d^2P}{d^2\phi}\right|_{\theta=K/\gamma} = \left\{\frac{7}{64\pi}\frac{e^2}{\varepsilon_0 c}\gamma^4 K\omega_u\frac{I}{e}\right\} NG_H(K)\ , \tag{6.8}$$

with

$$G_H(K) = \frac{K\left(K^6 + K^4 + \frac{3}{7}K^2 + \frac{1}{14}\right)}{\left(\frac{1}{4} + K^2\right)^{7/2}}\ . \tag{6.9}$$

Equations (6.8) and (6.9) correspond respectively to Eqs. (5.18) and (5.19). The function $G_H(K)$ is plotted in Fig. 6-1. The angular function $g_K^H(\theta)$ is normalized so that $g_K^H(\theta = K/\gamma) = 1$. For a general angle, it is given by

$$g_K^H(\theta) = \frac{(1+4K^2)^{7/2}}{(1+6K^2+14K^4+14K^6)} \frac{[(A^2+2B^2)(A^2-4B^2) - 2\gamma^2\theta^2(A^2+B^2)]}{(A^2-4B^2)^{7/2}} , \tag{6.10}$$

where

$$A = K^2 + \gamma^2\theta^2 + 1 , \quad B = K\gamma\theta . \tag{6.11}$$

The angular function is plotted in Fig. 6.2 as a function of $\gamma\Delta\theta = \gamma(\theta - K/\gamma)$. In the limit K becomes large, it approaches to the function

$$g_K^H(\theta) \rightarrow \frac{1}{(1+(\gamma\Delta\theta)^2)^{5/2}} + \frac{5}{7}\frac{(\gamma\Delta\theta)^2}{(1+(\gamma\Delta\theta)^2)^{7/2}} . \tag{6.12}$$

This becomes the same as the angular function of the bending magnet radiation if one identifies $\Delta\theta = \psi$. In the limit K vanishes, on the other hand,

$$g_K^H(\theta) \rightarrow \frac{1+(\gamma\theta)^4}{(1+\gamma^2\theta^2)^5} . \tag{6.13}$$

REFERENCES

[1] J. Schwinger, Phys. Rev. 75, 1912, (1949).

[2] R.P. Feynman, *The Feynman Lecture on Physics* (Addison- Wesley Pub. Co.,), (1963).

[3] S. Krinsky, M.L. Perlman, and R.E. Watson, In *Handbook on Synchrotron Radiation*, edited by E.E. Koch (North-Holland Publ. Co., Amsterdam), Chap. 2, (1983).

[4] A. Hofmann, Stanford Synchrotron Radiation Laboratory ACD-Note 38, (1986).

[5] K.-J. Kim, "Characteristics of Synchrotron Radiation," Physics of Partical Accelerators, 184, AIP Conference Proceedings, American Institute of Physics, New York, page 565, (1989).

[6] G.K. Green, Brookhaven National Laboratory Report BNL-50522, (1976).

[7] K.-J. Kim, Nucl. Instr. Methods **A246**, 71, (1986).

[8] R. Coisson, In *European Synchrotron Radiation Facility, The Machine*, edited by D.J. Thompson and M.W. Poole (ESF Strasbourg), 57, (1979).

[9] R. Halbach, J. Phys. (Paris) **44**, C1-211, (1983).

[10] D.F. Alferov, Yu. A. Bashmakov, and E.G. Bessonov, Zh. Tekh. Fiz. **43**, 2126; English translation in Sov. Phys. Tech. Phys. **18**, 1336, (1974), (1973).

[11] S. Krinsky, IEEE Trans Nucl. Science **NS-30**, 3078, (1983).

[12] K.-J. Kim, in *X-ray Data Booklet*, edited by D. Vaughn, Lawrence Berkeley Laboratory, Pub-490 Rev, (1986).

[13] B.M. Kincaid, J. Optical Soc. Am. B2, (1985).

[14] K.-J. Kim, Proceedings of 1987 Particle Accelerator Conf., IEEE Catalogue No. CH2387-9/87, 194, (1987).

[15] K.-J. Kim, Nucl. Instr. Methods **A246**, 67, (1986).

[16] A. Hofmann, Nucl. Instr. Methods **152**, 17, (1978).

[17] S. Sasaki, S. Hashimoto, H. Kobayashi, M. Takao and Y. Miyahara, Conceptual Design of Quasi-Periodic Undulator, JAERI - Memo 06-227, (1994).

[18] M. Moissev, M. Nikitin and F. Fedorov, Sov. Phys. J. 21, 332, (1978).

[19] K.-J. Kim, Nucl. Instr. Meth. 219, 425, (1984).

[20] J. Goulon, P. Elleaume and D. Rauox, Nucl. Instr. Meth. A254, 192, (1987).

[21] H. Onuki, Nucl. Instr. Meth. A291, 371, (1990).

[22] P. Elleaume, Nucl. Inst. Meth. A291, 371, (1990).

[23] S. Yamamoto and H. Kitamura, Japanese J. of Appl. Phys. 26, L1613.

[24] S. Sasaki, K. Miyata and T. Takada, Japanese J. of Appl. Physics, 31 ; L 1794, (1992).

[25] D.F. Alferov, Yu. A. Bashmakov, and E.G. Bessonov, 1976, Zh. Tekh. Fiz. **46**, 2392: English translation in Sov. Phys. Tech. Phys. **21**, 1408, (1976).

[26] B.M. Kincaid, J. Appl. Phys. **48**, 2684, (1977).

[27] K.-J. Kim, to be published.

Figure Captions

Figure 1-1 Comparison of spectral characteristics of bending magnet, wiggler and undulator radiation.

Figure 2-1 Average spectral brightness with a 0.1% bandwidth, as a function of photon energy, for a variety of synchrotron radiation sources. For each undulator, the brightness curve is the envelope of two or more harmonics.

Figure 3-1 The functions $G_1(y)$ and $H_2(y)$, where y is the ratio of photon energy to critical photon energy.

Figure 3.2 The angular spread of bending magnet radiation times γ as a function of ω/ω_c.

Figure 3-3 Normalized intensities of horizontal and vertical polarization components, as functions of the vertical observation angle ψ, for different photon energies. (Adapted from Green , [6].)

Figure 4-1 Schematic drawing of a periodic magnet structure (an undulator or wiggler) of period λ_u and with a number of periods, N.

Figure 4-2 The phase space distribution of wiggler radiation as a superposition of contributions from different poles.

Figure 5-1 The angular distribution of fundamental (n=1) undulator radiation for the limiting case of zero beam emittance. The x and y axes correspond to the observation angles θ and ψ (in radians), respectively, and the z axis is is the intensity in photons $\cdot s^{-1} \cdot amp^{-1} \cdot (0.1\ mr)^{-2} \cdot (1\%\ bandwidth)^{-1}$. The undulator parameters for this theoretical calculations were N = 14.K = 1.87 λ_u = 3.5 cm, and E = 1.3 GeV. (Figure courtesy of R. Tatchyn, SLAC.

Figure 5-2 The function $F_{n(}K)$ for various values of n, where K is the deflection parameter.

Figure 5-3 The function $Q_n(K)$ for various values of n.

Figure 5-4 Coherent fraction, i.e., the fraction of the flux that is transversely coherent. The solid curve is the full coherent fraction, while the dotted line is the vertical coherent fraction.

Figure 5-5 The function G (K) representing the interference effect in the angular distribution of the power from a planar undulator.

Figure 5-6 The angular function $f_K(\phi,\psi)$, for various values of the deflection parameter K: (a) as a function of the vertical observation angle ψ when the horizontal observation angle $\phi = 0$ and (b) as a function of ϕ when $\psi = 0$.

Figure 6-1 The function $G_H(K)$ representing the interference effect in the angular distribution of the power from a helical undulator.

Figure 6-2 The angular function $g_K^H(\theta)$ for various values of K.

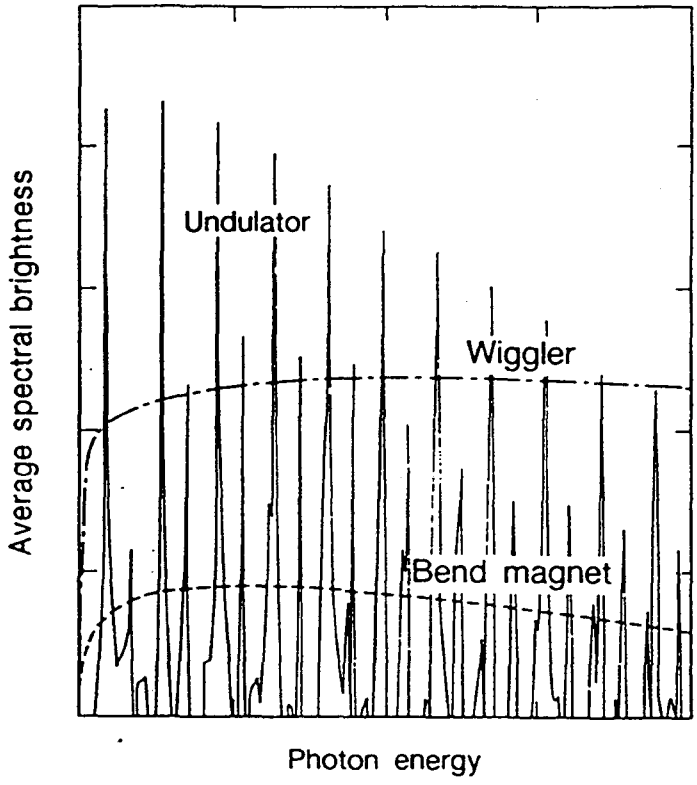
Average spectral brightness
Undulator
Wiggler
Bend magnet
Photon energy

Figure 1-1

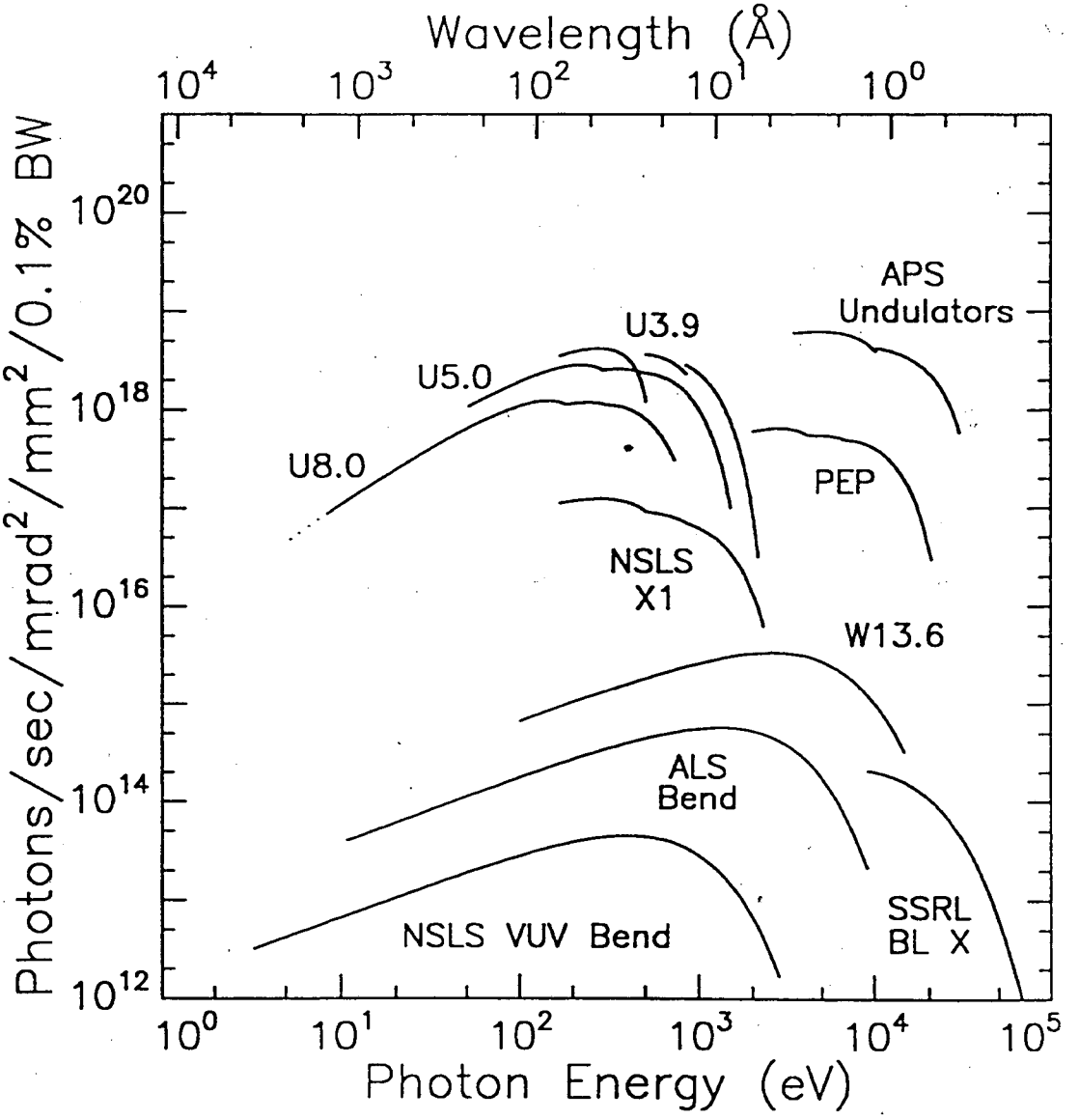
Wavelength (Å)
10^4
10^3
10^2
10^1
10^0
Photons/sec/mrad^2/mm^2/0.1% BW
10^{20}
10^{18}
10^{16}
10^{14}
10^{12}
APS
Undulators
U3.9
U5.0
U8.0
PEP
NSLS
X1
W13.6
ALS
Bend
NSLS VUV Bend
SSRL
BL X
10^0
10^1
10^2
10^3
10^4
10^5
Photon Energy (eV)

Figure 2-1

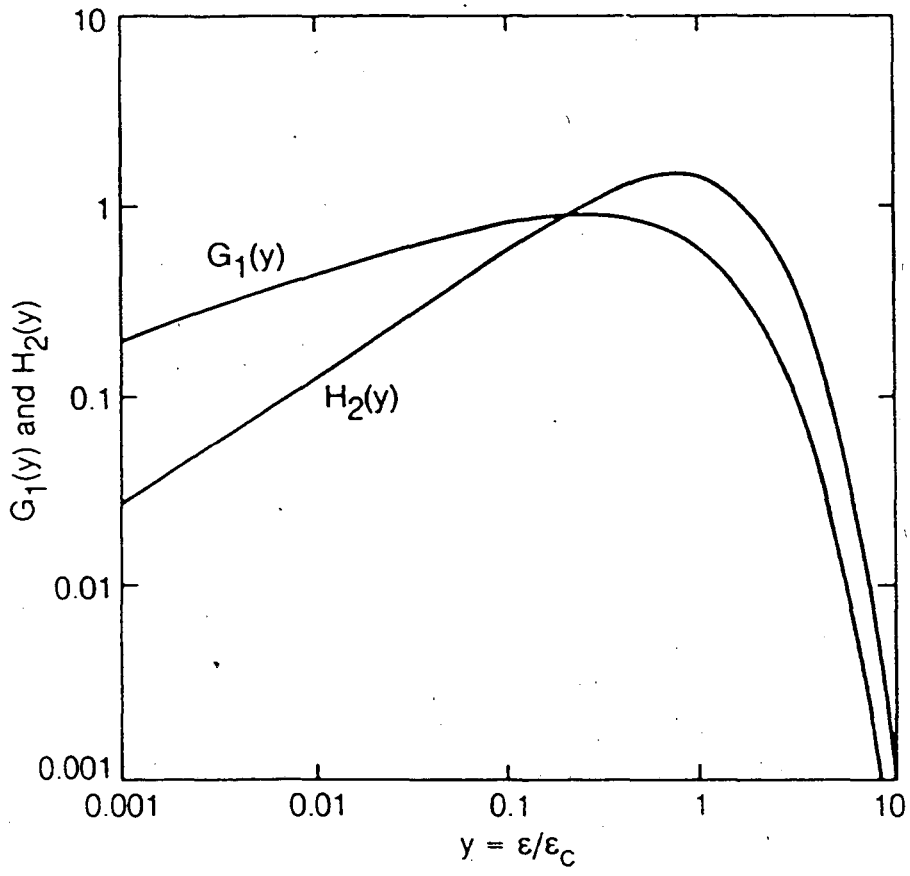
10
1
0.1
0.01
0.001
$G_1(y)$
$H_2(y)$
$G_1(y)$ and $H_2(y)$
0.001
0.01
0.1
1
10
$y = \varepsilon/\varepsilon_c$

Figure 3-1

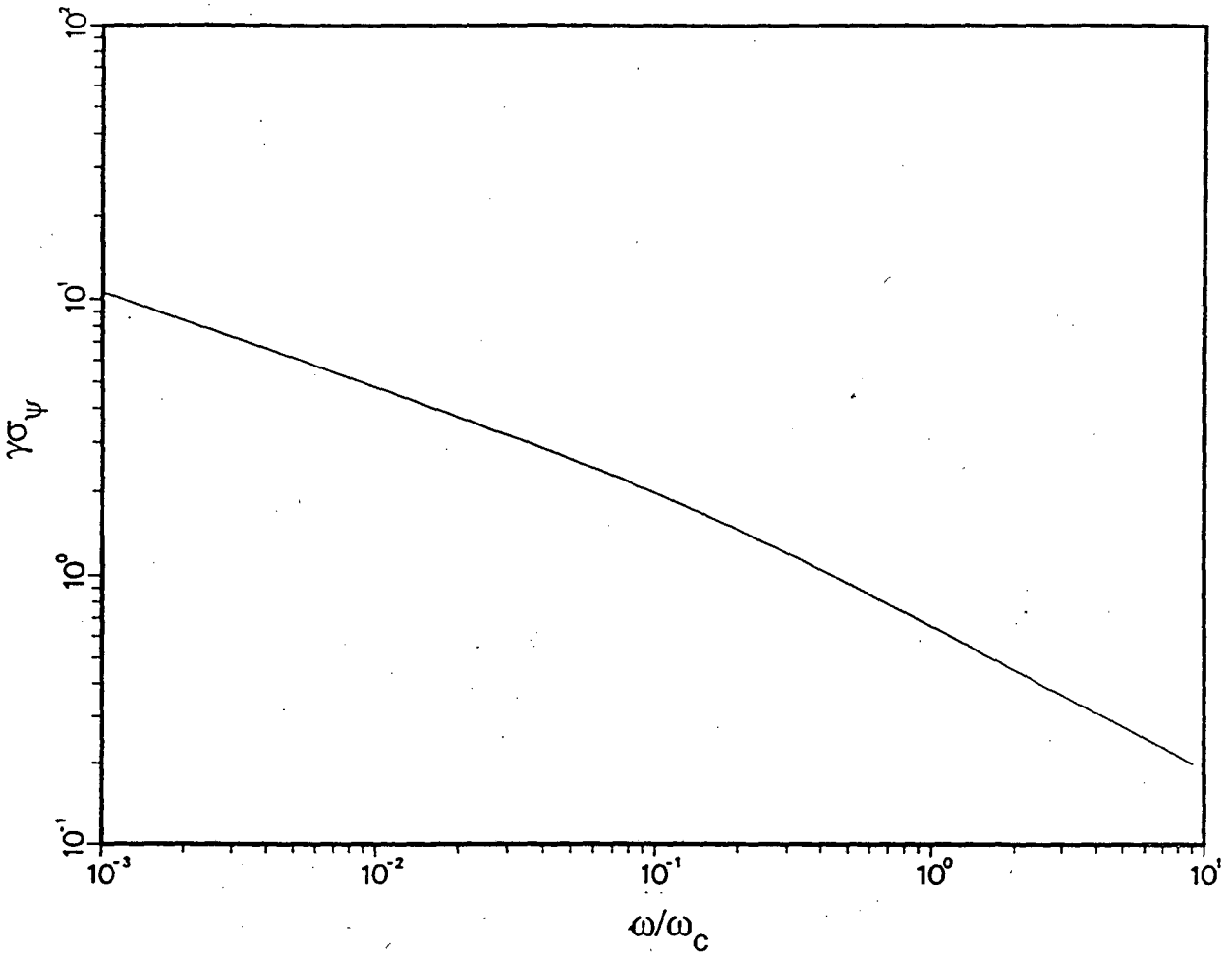
10^2
10^1
10^0
10^{-1}
$\gamma\sigma_\psi$
10^{-3}
10^{-2}
10^{-1}
10^0
10^1
ω/ω_c

Figure 3-2

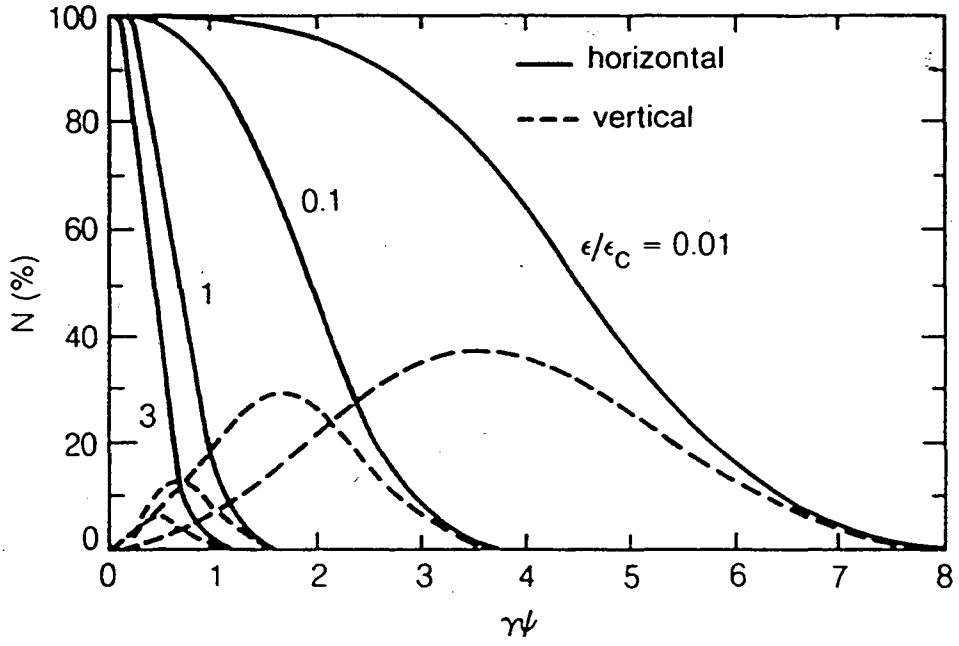
100
80
60
40
20
0
N (%)
0
1
2
3
4
5
6
7
8
γψ
horizontal
vertical
0.1
1
3
ε/εc = 0.01

Figure 3-3

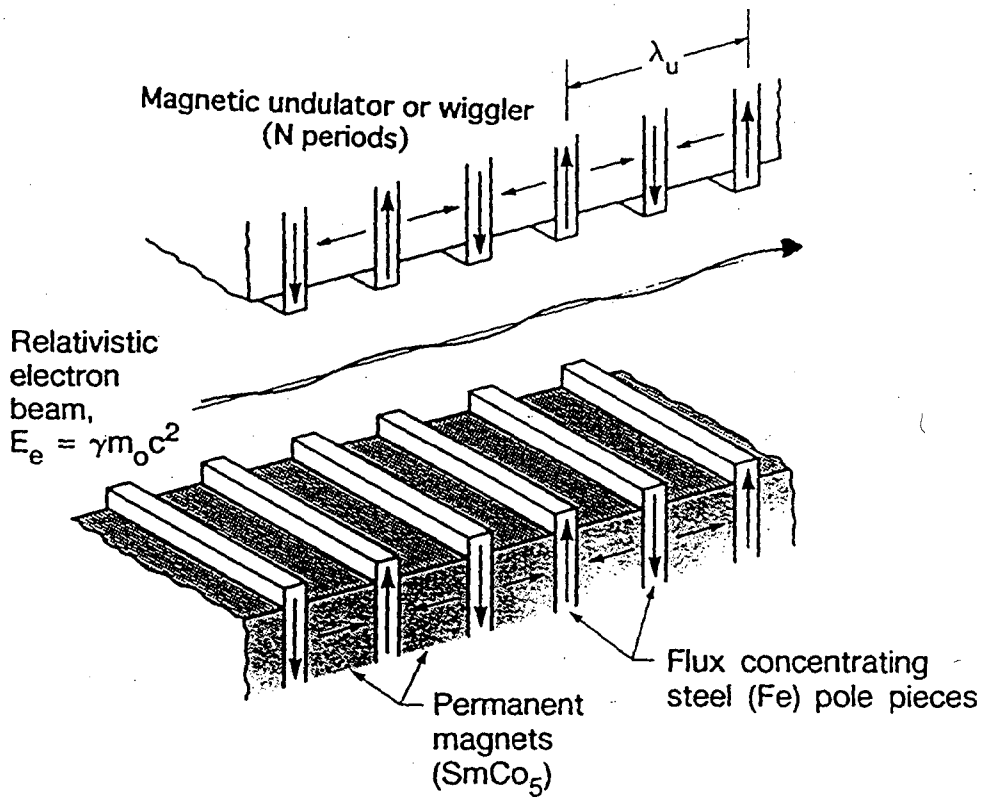
λ_u
Magnetic undulator or wiggler
(N periods)
Relativistic
electron
beam,
$E_e = \gamma m_o c^2$
Flux concentrating
steel (Fe) pole pieces
Permanent
magnets
($SmCo_5$)

Figure 4-1

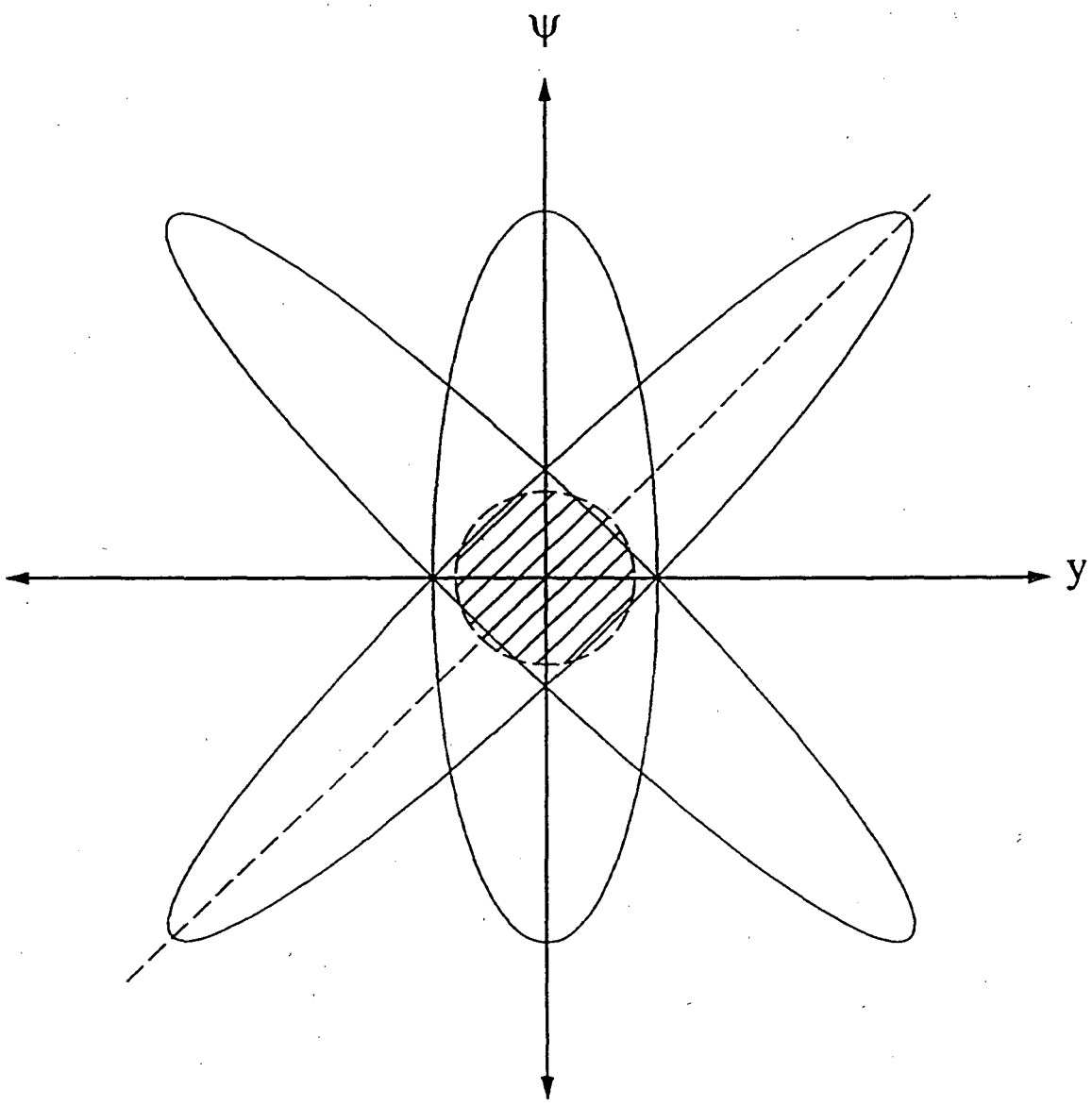

Figure 4-2

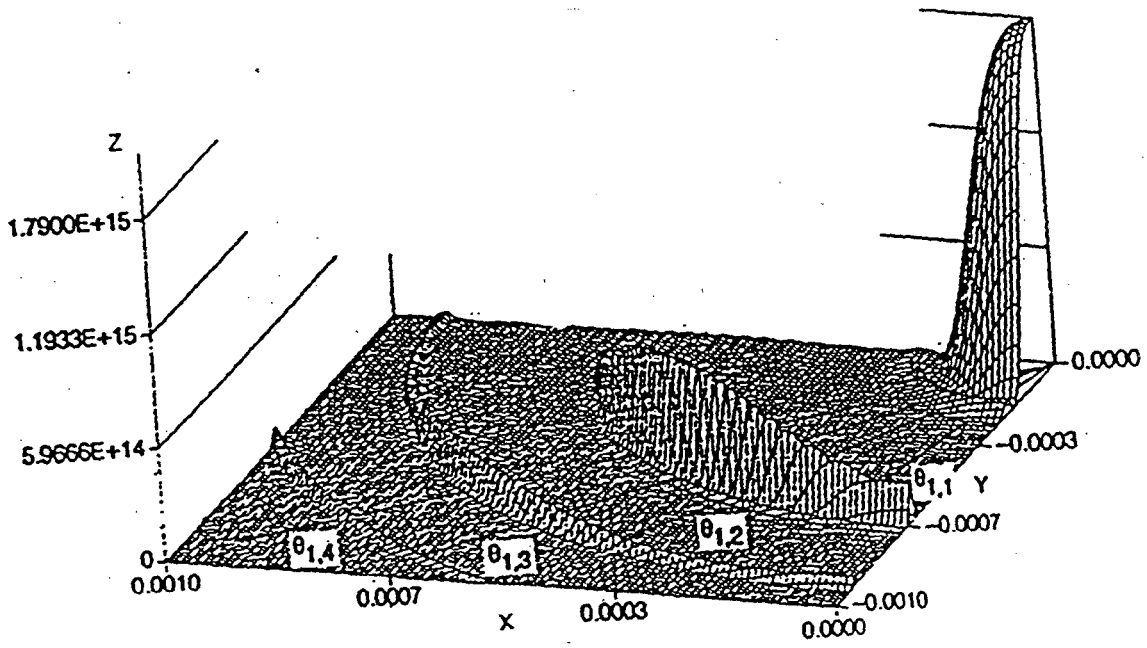
Z
1.7900E+15
1.1933E+15
5.9666E+14
0
0.0010
0.0007
0.0003
0.0000
X
θ1,4
θ1,3
θ1,2
θ1,1
Y
0.0000
-0.0003
-0.0007
-0.0010

Figure 5-1

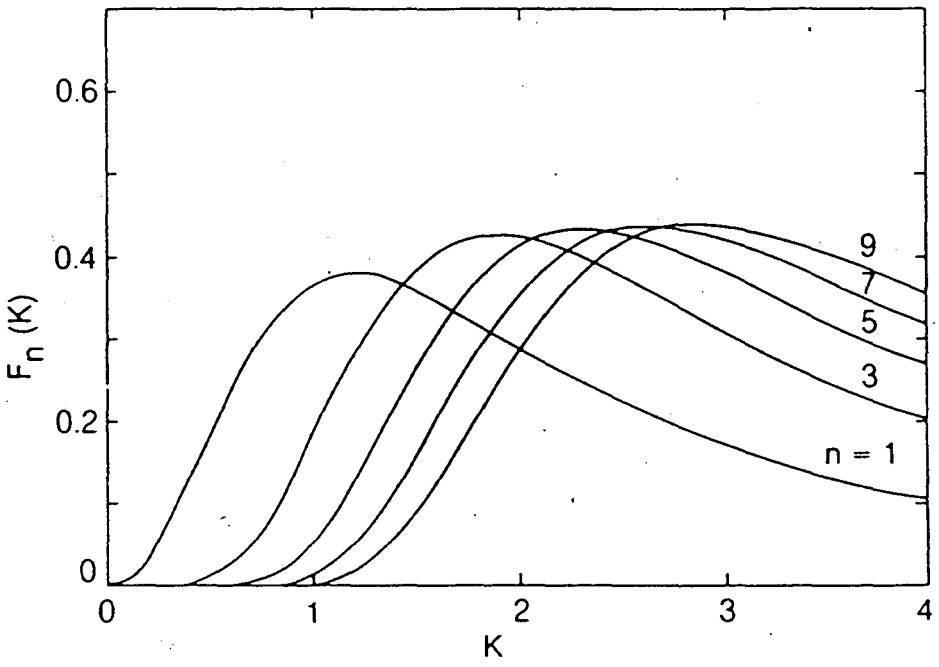

Figure 5-2

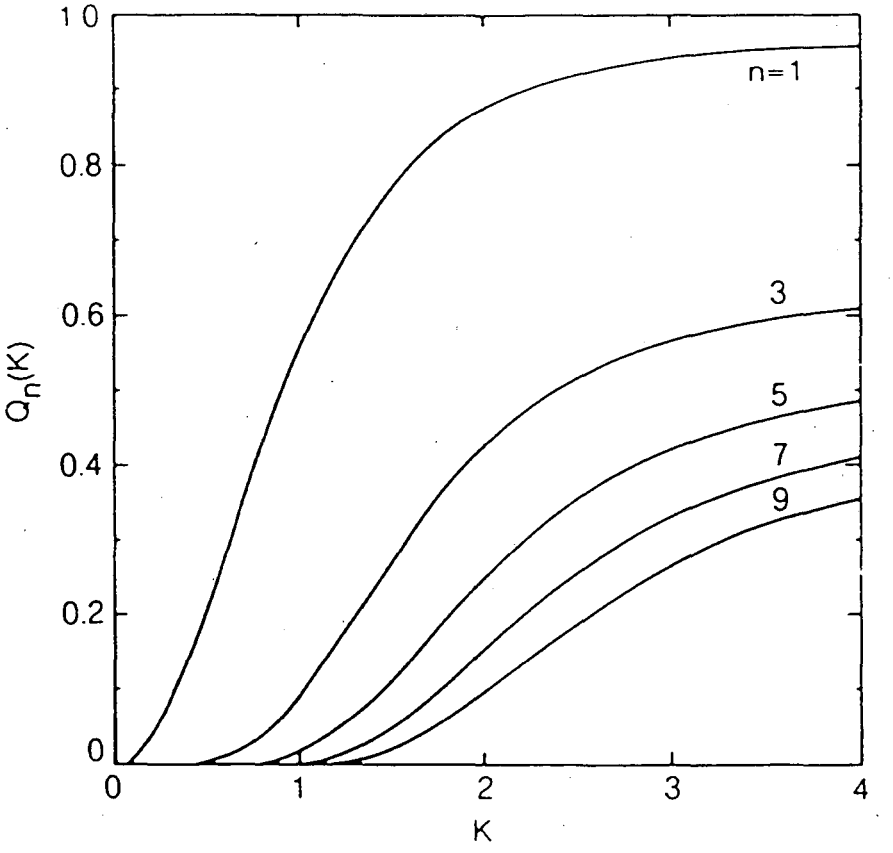

Figure 5-3

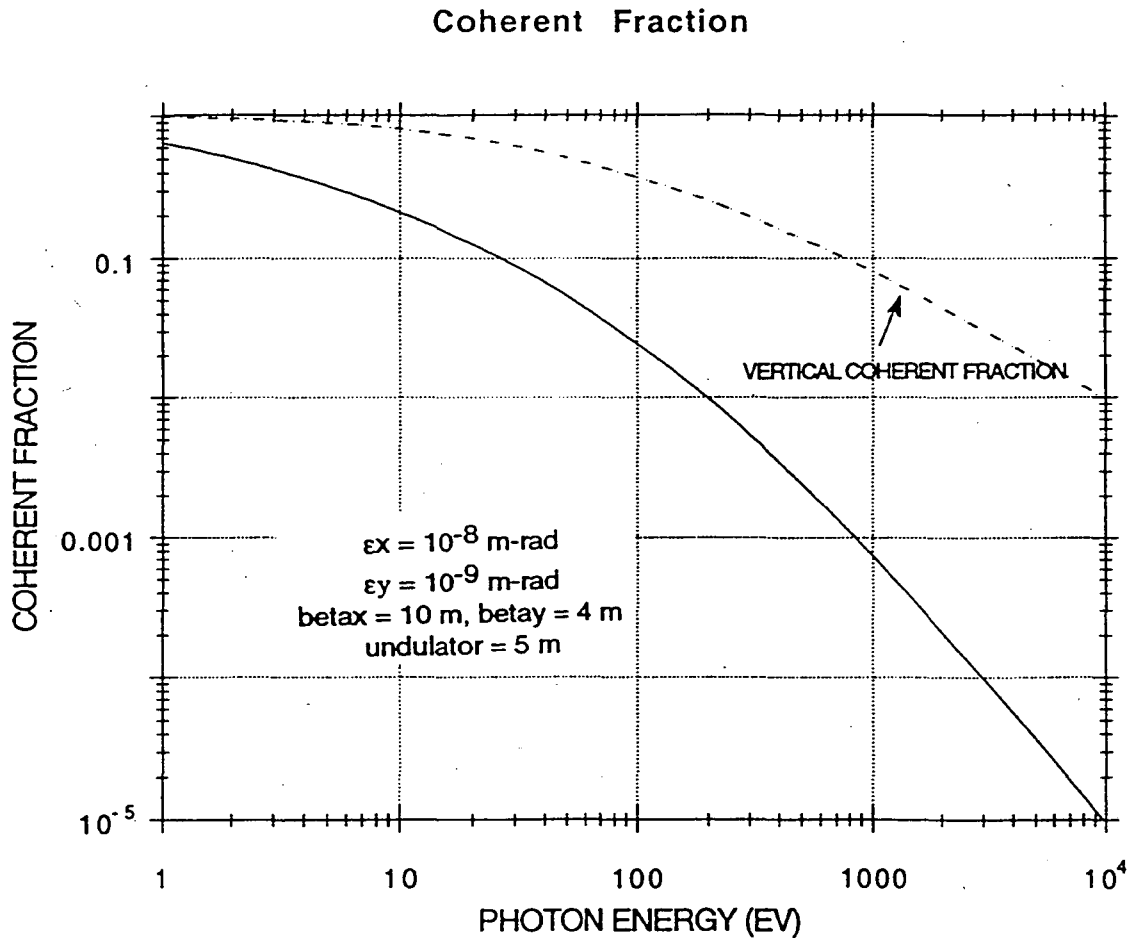
Coherent Fraction
COHERENT FRACTION
0.1
0.001
10^-5
VERTICAL COHERENT FRACTION
εx = 10^-8 m-rad
εy = 10^-9 m-rad
betax = 10 m, betay = 4 m
undulator = 5 m
1
10
100
1000
10^4
PHOTON ENERGY (EV)

Figure 5-4

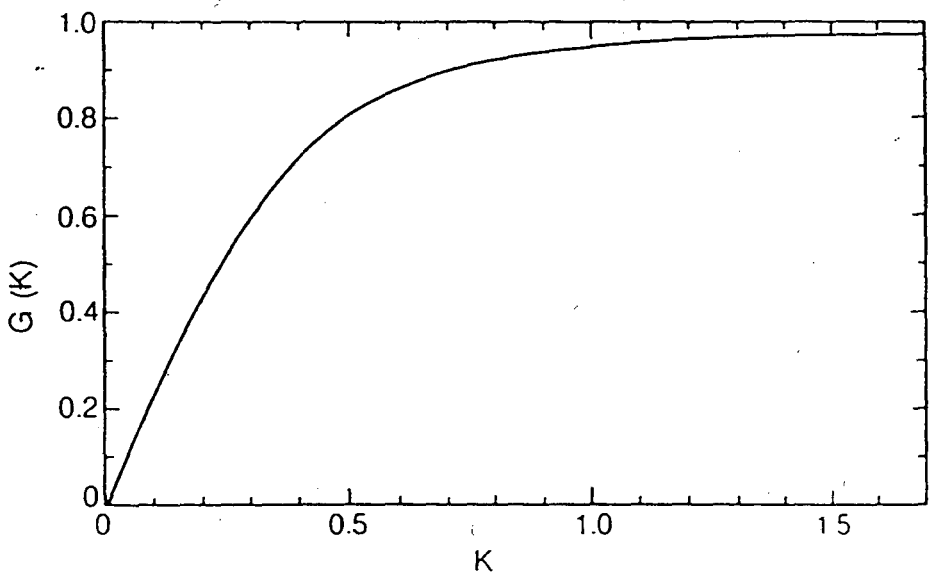

Figure 5-5

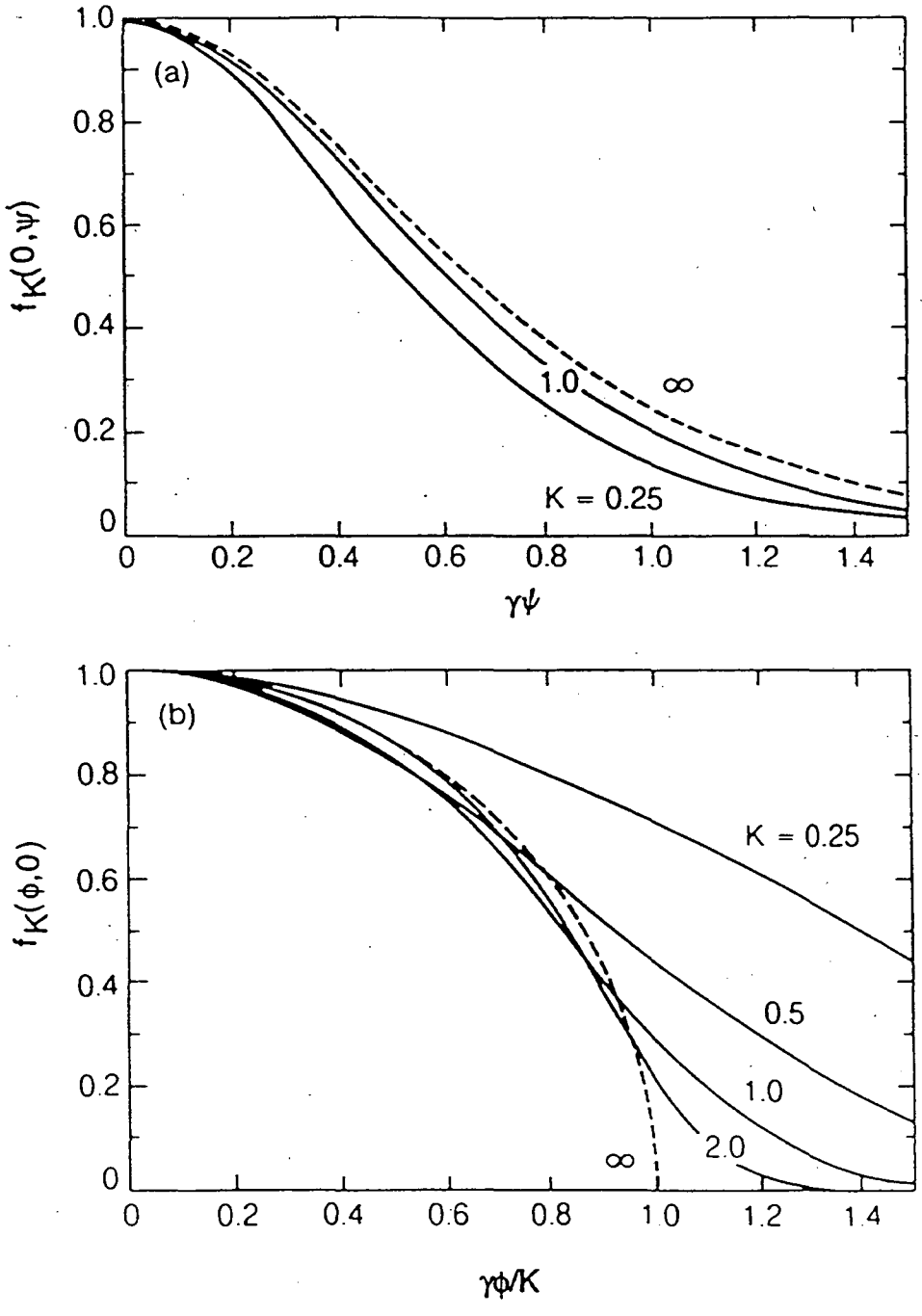

Figure 5-6

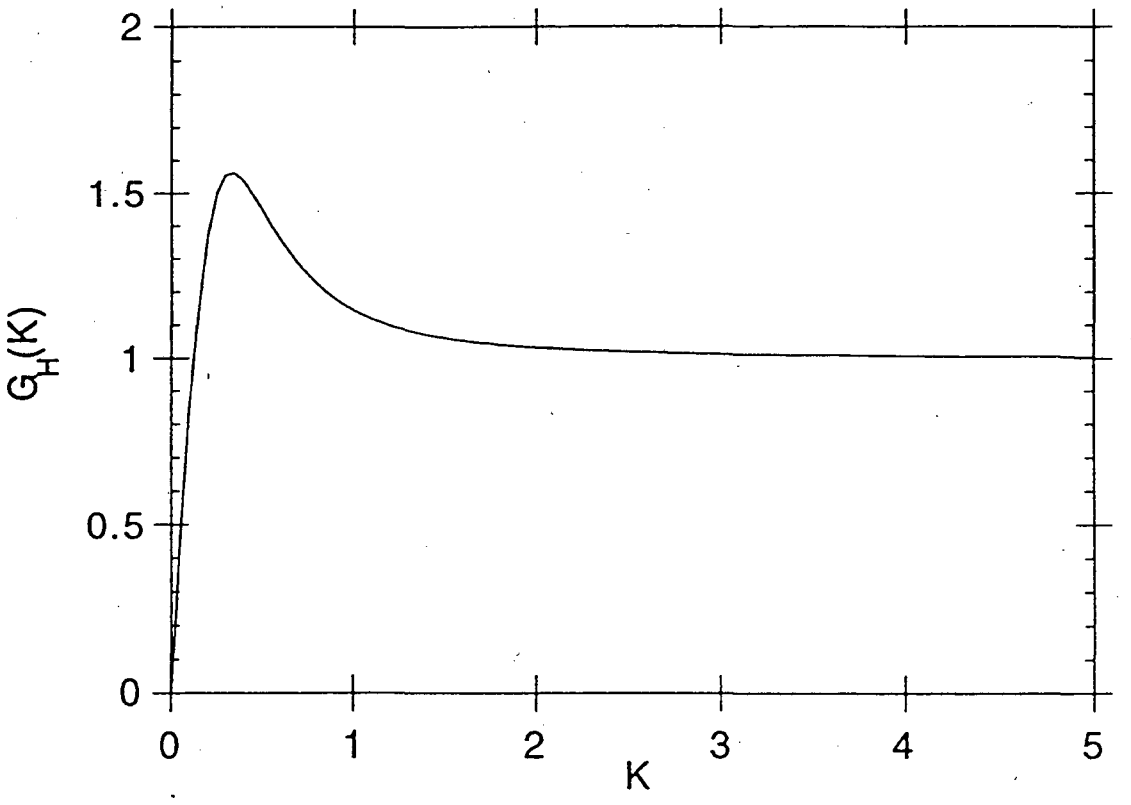

Figure 6-1

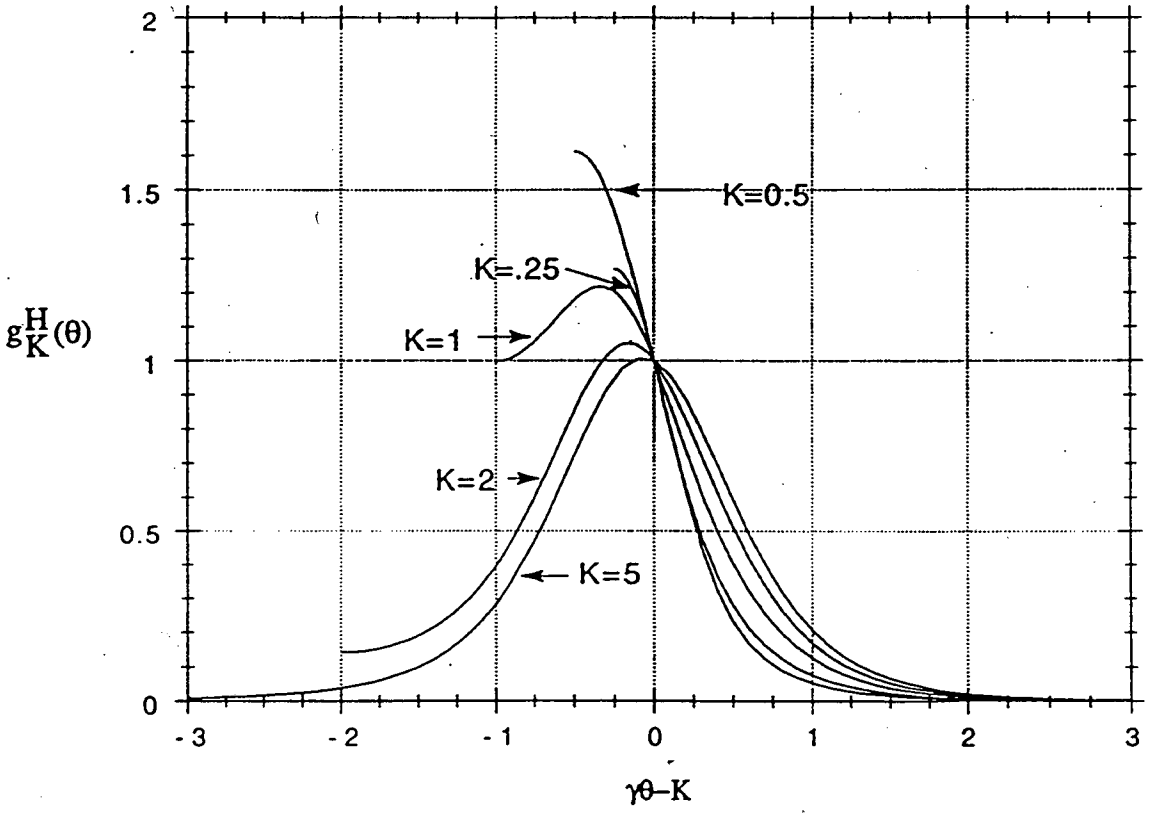

Figure 6-2

LAWRENCE BERKELEY LABORATORY
UNIVERSITY OF CALIFORNIA
TECHNICAL AND ELECTRONIC
INFORMATION DEPARTMENT
BERKELEY, CALIFORNIA 94720